JACS
JOURNAL OF THE AMERICAN CHEMICAL SOCIETY

Communication

pubs.acs.org/JACS

Efficient Planar Perovskite Solar Cells Based on 1.8 eV Band Gap $CH_3NH_3PbI_2Br$ Nanosheets via Thermal Decomposition

Yixin Zhao*[,†] and Kai Zhu*[,‡]

[†]School of Environmental Science and Engineering, Shanghai Jiao Tong University, 800 Dongchuan Road, Shanghai 200240, China

[‡]Chemical and Materials Science Center, National Renewable Energy Laboratory, 15013 Denver West Parkway, Golden, Colorado 80401, United States

Supporting Information

ABSTRACT: Hybrid organometallic halide perovskite $CH_3NH_3PbI_2Br$ (or $MAPbI_2Br$) nanosheets with a 1.8 eV band gap were prepared via a thermal decomposition process from a precursor containing PbI_2, MABr, and MACl. The planar solar cell based on the compact layer of $MAPbI_2Br$ nanosheets exhibited 10% efficiency and a single-wavelength conversion efficiency of up to 86%. The crystal phase, optical absorption, film morphology, and thermogravimetric analysis studies indicate that the thermal decomposition process strongly depends on the composition of precursors. We find that MACl functions as a glue or soft template to control the initial formation of a solid solution with the main $MAPbI_2Br$ precursor components (i.e., PbI_2 and MABr). The subsequent thermal decomposition process controls the morphology/surface coverage of perovskite films on the planar substrate and strongly affects the device characteristics.

During the past two years, the world has witnessed rapid development of a new solar cell technology based on lead halide perovskites (e.g., $CH_3NH_3PbI_3$ or $MAPbI_3$) with various device configurations.[1−10] Besides the exceptional high efficiency (certified 17.9%) and simple solution fabrication process, halide perovskites are also capable of band gap tuning from about 1.5 to 2.2 eV by changing the composition of perovskites (e.g., substitution of I with Br ions).[11,12] Seok et al. initially demonstrated the deposition of $MAPb(I_{1-x}Br_x)_3$ in mesoporous TiO_2 films with reasonable device performance (especially for the composition where $x \approx 0.2$).[11] Hodes et al. investigated $MAPbBr_3$-based cells with relatively high open-circuit voltage (V_{oc}) under one-sun illumination.[13,14] Also using $MAPbBr_3$ as the absorber, Seok et al. recently achieved a remarkable 6.7%-efficient device with a V_{oc} of 1.40 V.[15] Moreover, Snaith et al. demonstrated band gap tuning with mixed organic cations (i.e., $CH_3NH_3^+$ and $HC(NH_2)_2^+$).[16] These band-gap-tunable perovskites could be promising for high-efficiency tandem solar cells in conjunction with other photovoltaic (PV) technologies (e.g., Si and CIGS). It is even possible to fabricate all-perovskite-based tandem (or multijunction) solar cells. It has been previously shown that a 1.8 eV top cell is suitable for tandem cells based on band-gap-tunable III−V semiconductors.[17] Among the perovskite family, $MAPbI_2Br$ has a band gap of ∼1.8 eV, which makes it a promising candidate for developing high-efficiency perovskite-based tandem solar cells.

Two common device architectures are usually used for constructing perovskite solar cells, i.e., mesoporous and planar structures. The mesoporous cell structure involves a layer of mesoporous metal oxide film (e.g., TiO_2, ZrO_2, Al_2O_3) that is coated/filled with perovskites. In contrast, the planar cell uses a thin layer of perovskite sandwiched between the electron- and hole-transport layers. The planar structure of perovskite cells is similar to the conventional thin-film PV technologies. Compared to the mesoporous cell structure, the planar perovskite cell is expected to be relatively easier for incorporation (especially as the top cell) to build tandem perovskite devices. Thus, developing a facile synthetic approach for preparing high-quality $MAPbI_2Br$ thin films would facilitate the development of perovskite-based tandem cells. Until now, only a few papers have reported on mesoporous perovskite cells using $MAPbI_{3-x}Br_x$ with x being close to 1. In these cells, photovoltage is usually limited to ∼0.8 V.[12]

Here, we report on the development and characterization of planar perovskite $MAPbI_2Br$ thin-film solar cells comprising a uniform, compact layer of $MAPbI_2Br$ nanosheets. These devices exhibit an overall energy conversion efficiency of ∼10% and a single-wavelength conversion efficiency of up to 86%. $MAPbI_2Br$ is prepared by thermal decomposition from a film deposited using a precursor containing PbI_2, MABr, and MACl. Although MACl is used in the precursor solution, the final product is $MAPbI_2Br$ without any traceable Cl, as determined by energy-dispersive X-ray (EDX) analysis. The structure evolution of $MAPbI_2Br$ formation from the thermal decomposition process during annealing is characterized by X-ray diffraction (XRD), UV−vis absorption, and scanning electron microscopy (SEM). We find that the thermal decomposition step not only affects the phase evolution of $MAPbI_2Br$ but also controls the final morphology/surface coverage of perovskite films on the planar substrate. The film morphology strongly affects the device characteristics of perovskite $MAPbI_2Br$ solar cells.

Figure 1a shows that the SEM image of $MAPbI_2Br$ film prepared from a precursor containing equimolar PbI_2 and MABr (denoted as the PbI_2+MABr precursor). The film is composed of large, belt-shape crystals with micrometer-sized uncovered areas on the substrate (a compact TiO_2 layer on fluorine-doped SnO_2 glass, denoted as c-TiO_2/FTO). Such film morphology is similar to the $MAPbI_3$ films deposited on c-TiO_2/FTO using a standard precursor containing equimolar PbI_2 and MAI.[6,18,19] The

Received: July 15, 2014
Published: August 13, 2014

dx.doi.org/10.1021/ja5071398 | J. Am. Chem. Soc. 2014, 136, 12241−12244

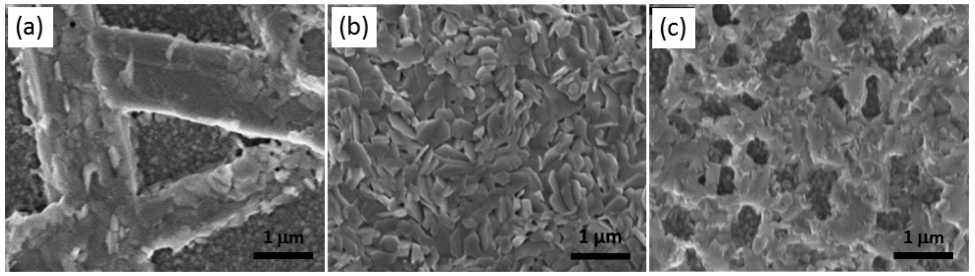

Figure 1. Typical SEM images of $MAPbI_2Br$ films deposited on c-TiO_2/FTO substrates from various precursor solutions: (a) PbI_2+MABr; (b) PbI_2+MABr+MACl; and (c) PbI_2+MABr+2MACl.

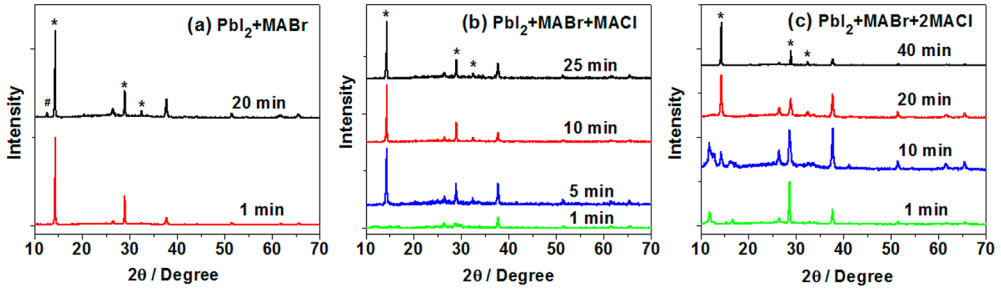

Figure 2. Effect of annealing time (as indicated) at 125 °C on the XRD patterns of $MAPbI_2Br$ films deposited on c-TiO_2/FTO substrate from various precursor solutions: (a) PbI_2+MABr; (b) PbI_2+MABr+MACl; and (c) PbI_2+MABr+2MACl. The main PbI_2 peak at 12.6° is labeled with a sharp sign. Asterisks denote the main perovskite peaks at about 14.4°, 29.0°, and 32.6°, corresponding to the (110), (220), and (310) planes, respectively. The other peaks are associated with the TiO_2/FTO substrates.

formation of large perovskite crystals and low surface coverage could be ascribed to the quick formation of $MAPbI_2Br$ on c-TiO_2/FTO. The $MAPbI_2Br$ crystal belts form on c-TiO_2/FTO immediately after the evaporation of the solvent dimethylformamide (DMF) even without annealing. Further annealing does not affect the morphology of $MAPbI_2Br$ belts. We also investigated the effect of adding MACl with different amounts to the PbI_2+MABr precursor on the properties of perovskite films. The new precursors contain PbI_2, MABr, and MACl with molar ratios of 1:1:1 or 1:1:2. For ease of comparison, these two precursors are called PbI_2+MABr+MACl and PbI_2+MABr +2MACl, respectively. The SEM images of the final $MAPbI_2Br$ films prepared from PbI_2+MABr+xMACl precursors are shown in Figure 1b,c, as indicated. When MACl is used in the precursor, the large belt-shape crystals (as seen with the PbI_2+MABr precursor) totally disappear and the c-TiO_2/FTO substrate is covered with small perovskite crystals. The $MAPbI_2Br$ film prepared from the PbI_2+MABr+2MACl precursor comprises interconnected small crystals with ~80%−90% surface coverage (Figure 1c), which is similar to a previous report on perovskite $MAPbI_{3-x}Cl_x$ for high-efficiency perovskite solar cells.[20] Most interestingly, when the PbI_2+MABr+MACl precursor is used, the $MAPbI_2Br$ film shows complete coverage on c-TiO_2/FTO with a compact layer of perovskite nanosheets (Figure 1b; the SEM image of this film on a larger scale/at lower magnification is shown in Figure S1 in the Supporting Information (SI)). The coverage of $MAPbI_2Br$ nanosheets is comparable to that of the $MAPbI_3$ films deposited by two-step methods.[21,22]

The optical absorption (UV−vis) properties of $MAPbI_2Br$ films prepared with various precursors are shown in Figure S2, which also shows that when the PbI_2+MABr precursor is used, the $MAPbI_2Br$ film turns to brown during the first minute of annealing at 125 °C. We use the term PbI_2·MABr·xMACl to describe the films prepared from PbI_2+MABr+xMACl precursors because the exact chemical and crystal structures of the compounds prepared from the MACl-added precursors during the early stages of annealing are unclear. The perovskite films deposited from these precursors slowly turn from yellowish to brown with much longer transition times at 125 °C. The UV−vis absorption study of the PbI_2·MABr·xMACl (x = 1 or 2) films with different annealing times (Figure S2b, S2c) reveals that it takes about 25 and 40 min at 125 °C for the yellowish PbI_2·MABr·MACl and PbI_2·MABr·2MACl films to evolve to the brown $MAPbI_2Br$ films, respectively. The absorbance of the final films prepared from PbI_2+MABr+xMACl precursors are stronger than that prepared from the PbI_2+MABr precursor.

Figure 2a compares the XRD patterns of $MAPbI_2Br$ films prepared from three different precursors. When no MACl is used, the characteristic diffraction peaks[12] at about 14.4° and 29.0° confirm the formation of $MAPbI_2Br$ during the initial 1 min annealing. The observed rapid crystallization process is consistent with previous reports on $MAPbI_2Br$ or similar perovskite compositions grown on mesoporous TiO_2 films.[11,12] When this film is further annealed for a longer time (20 min), the characteristic PbI_2 (001) peak at ~12.6° is observed along with the perovskite peaks, suggesting that a partial decomposition of $MAPbI_2Br$ into PbI_2 occurs with long annealing duration. Figure 2b and 2c show the time-dependent XRD evolution of PbI_2·MABr·MACl and PbI_2·MABr·2MACl films, respectively. For both films, the characteristic $MAPbI_2Br$ peak at 14.4° cannot be observed during the initial 1 min annealing. The main 14.4° peak slowly develops after elongated annealing. A longer annealing time is required to form perovskite $MAPbI_2Br$ when using a higher content of MACl in the precursor. The crystal evolution of $MAPbI_2Br$ from PbI_2·MABr·xMACl is consistent with their UV−vis spectra evolution under 125 °C annealing.

Figure 3 shows the photocurrent density−photovoltage (J−V) curves of perovskite $MAPbI_2Br$-based planar solar cells. In these solar cells, the $MAPbI_2Br$ layer is deposited on the c-TiO_2/FTO substrate and covered with the spiro-MeOTAD/Ag hole

dx.doi.org/10.1021/ja5071398 | J. Am. Chem. Soc. 2014, 136, 12241−12244

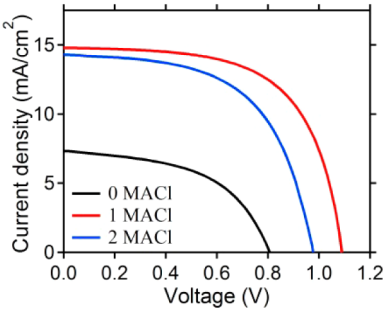

Figure 3. Photocurrent density−photovoltage (J−V) curves of perovskite solar cells prepared from different precursor compositions (i.e., PbI_2+MABr or 0 MACl; PbI_2+MABr+MACl or 1 MACl; and PbI_2+MABr+2MACl or 2 MACl).

extraction contact. When the PbI_2+MABr precursor is used, the belt-shaped $MAPbI_2Br$-based cell exhibits poor (3.06%) device performance with a low short-circuit photocurrent density (J_{sc}) of 7.34 mA/cm^2, V_{oc} of 0.80 V, and fill factor (FF) of 0.52. This is similar to the performance level of either a previously reported $MAPbI_2Br$-based cell or the device based on $MAPbI_3$ film with similar film morphology.[12,18] The solar cell using $MAPbI_2Br$ with ∼80%−90% coverage prepared from the PbI_2+MABr+2MACl precursor shows much enhanced cell performance (∼8%) with improvement for all PV parameters (J_{sc}, 14.30 mA/cm^2; V_{oc}, 0.98 V; and FF, 0.58). When using the compact $MAPbI_2Br$ nanosheet-based film prepared by the PbI_2·MABr·MACl route, the device performance is further improved to ∼10%. The details of the PV parameters of these devices are given in Table S1 (SI). It is noteworthy that the peak value of the incident photon-to-current efficiency (IPCE) of the $MAPbI_2Br$-nanosheet-based cell has reached up to 86% (Figure S3). The lower V_{oc} values for solar cells based on $MAPbI_2Br$ films with poorer coverage are likely caused by internal shunting at uncovered area. The recombination resistances and dark currents of these different $MAPbI_2Br$ solar cells are shown in Figures S4 and S5 (SI) with a clear correlation with the perovskite film coverage (Figure 1). The PbI_2·MABr·MACl-based $MAPbI_2Br$ film with nearly complete coverage shows lower dark current and higher recombination resistance than the other two film morphologies. This observation is consistent with recent reports for planar $MAPbI_{3-x}Cl_x$ solar cells that better perovskite coverage on the substrate leads to improved device performance.[16,23,24]

Because the crystal structure and chemical composition of the $MAPbI_2Br$ films prepared from all three precursors are the same, we attribute the observed difference in the device characteristics to the apparent difference in their film morphologies. Developing 1.55 eV band gap perovskites (e.g., $MAPbI_3$) with uniform film morphology and high surface coverage on the substrate has received significant worldwide attention for developing high-efficiency single-junction perovskite solar cells.[4,5,18,20,25−29] Understanding the perovskite growth mechanism and the correlation between the perovskite film morphology and device characteristics is critical to further enhance the energy conversion efficiency for single-junction perovskite cells and to develop wide-band-gap perovskites for tandem or multijunction perovskite solar cells. To explore the growth mechanism underlying the transition of the 1.8 eV $MAPbI_2Br$ from the initial PbI_2·MABr·MACl compound when using the PbI_2+MABr+MACl precursor, we carried out thermogravimetric analysis (TGA) on the thermal decomposition process of PbI_2·MABr·MACl. The TGA measurements of MACl, MABr, and $MAPbI_2Br$ are also conducted for comparison. We find that the MACl and MABr powders do not show any weight loss even when the temperature is about 150−175 °C (Figure 4a). In contrast, $MAPbI_2Br$ starts to

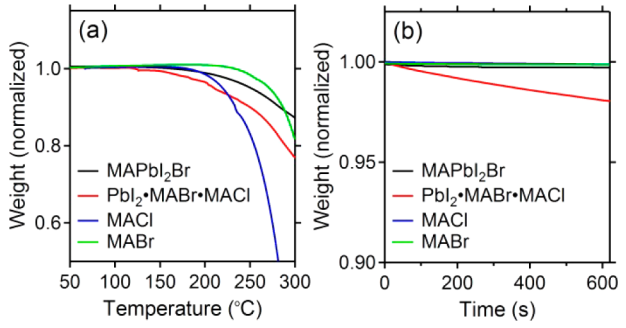

Figure 4. (a) Thermogravimetric analysis of MACl, MABr, $MAPbI_2Br$ and PbI_2·MABr·MACl (a) from 50 to 300 °C with a heating rate of 5 °C/min and (b) heated at 125 °C for 600 s.

lose weight near 150 °C, whereas PbI_2·MABr·MACl starts to lose weight at ∼125 °C. The lost weight contains both Cl and Br as determined from TGA with mass spectrometry (TGA-MS). These results suggest that both MABr and MACl do not exist as the impurity (or secondary phase) in their original form in the PbI_2·MABr·MACl compound. Presumably, MACl and MABr are incorporated in the crystal lattice of PbI_2·MABr·MACl in the form of MA^+, Br^-, and Cl^- as part of a solid solution or an alloy. These results suggest that MA^+/Br^- and MA^+/Cl^- can be released from $MAPbI_2Br$ or PbI_2·MABr·MACl at lower temperatures than their individual components, leading to the observed sublimation of MACl and MABr from $MAPbI_2Br$ and PbI_2·MABr·MACl at 125 and 150 °C, respectively. Figure 4b shows the time-dependent TGA results of MACl, MABr, $MAPbI_2Br$, and PbI_2·MABr·MACl annealed at 125 °C. It further confirms that MACl, MABr, and $MAPbI_2Br$ are thermally stable at 125 °C for 600 s. In contrast, PbI_2·MABr·MACl displays significant weight loss during annealing at 125 °C. Chlorine is found in the TGA-MS measurement, confirming that the weight loss is related to the sublimation of MACl. This TGA result is in agreement with the EDX analysis, where the Cl content is found to decrease with annealing at 125 °C. The results from TGA (Figure 4), XRD (Figure 2), and absorption (Figure S2) studies suggest that MACl sublimes from the crystal lattice of PbI_2·MABr·MACl during annealing at 125 °C. This thermal decomposition process eventually leads to the formation of $MAPbI_2Br$.

To understand the film morphology evolution during the thermal decompose process, we compared the SEM images of the PbI_2·MABr·MACl (Figure 5a,b) and PbI_2·MABr·2MACl (Figure 5c,d) films at the beginning and final stages of annealing at 125 °C. During the early stage (1 min) of annealing with the solvent (DMF) evaporation, both PbI_2·MABr·MACl and PbI_2·MABr·2MACl films are relatively compact, which significantly differs from the large belt-shape crystal formation observed for $MAPbI_2Br$ prepared from the PbI_2+MABr precursor. Thus, the incorporation of MACl in the PbI_2+MABr precursor helps to form a uniform layer, and MACl seems to function as a glue by forming PbI_2·MABr·xMACl. As a result, the PbI_2·MABr·MACl film with nearly complete coverage is coated on the c-TiO_2/FTO substrate. The PbI_2·MABr·2MACl film also exhibits uniform coverage on the substrate; however, some small pores are observed within the film. EDX analysis indicates that the amount of Cl in the film decreases with annealing duration. At the later

dx.doi.org/10.1021/ja5071398 | J. Am. Chem. Soc. 2014, 136, 12241−12244

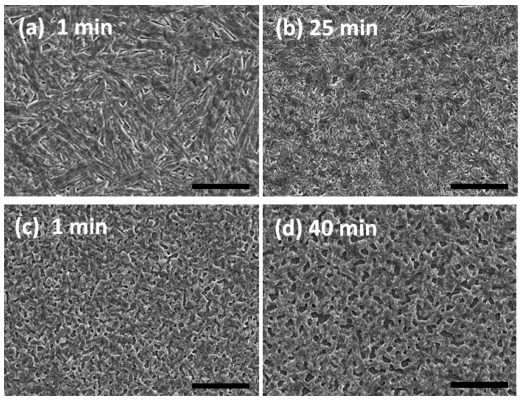

Figure 5. SEM images of (a,b) PbI_2·MABr·MACl and (c,d) PbI_2·MABr·2MACl films deposited on c-TiO_2/FTO substrate annealed at 125 °C for different times. The scale bar is 5 μm.

stage of annealing (Figure 5b,d), both PbI_2·MABr·MACl and PbI_2·MABr·2MACl films turn to $MAPbI_2Br$ without any traceable Cl. However, the final $MAPbI_2Br$ films by thermal decomposition of PbI_2·MABr·MACl and PbI_2·MABr·2MACl films with similar initial coverage show a significant difference in their film morphology. The $MAPbI_2Br$ film formed from PbI_2·MABr·MACl film consists of a compact packing of nanosheets completely covering the substrate, whereas the perovskite film developed from PbI_2·MABr·2MACl shows ~10% uncovered area. This morphology difference could be attributable to the different amount of MACl loss during the thermal annealing/decomposition from PbI_2·MABr·*x*MACl. In the case of PbI_2·MABr·2MACl, the relative large amount of MACl sublimation may cause the formation of many pores. On the other hand, the proper loss of MACl from the PbI_2·MABr·MACl helps the formation of the compact layer of $MAPbI_2Br$ nanosheets, in which the MACl behaves more like a soft template and glue.

In summary, we report on the development and characterization of planar perovskite thin-film solar cells based on a uniform, compact layer of 1.8 eV band gap $MAPbI_2Br$ nanosheets. $MAPbI_2Br$ is prepared by thermal decomposition from a film deposited using a precursor containing PbI_2, MABr, and MACl. The thermal decomposition process not only affects the phase evolution of $MAPbI_2Br$ but also controls the final morphology/surface coverage of perovskite films on the planar substrate; this, in turn, strongly affects the device characteristics of $MAPbI_2Br$ solar cells. Using this new synthetic approach, we obtain an overall energy conversion efficiency of ~10% and a single-wavelength conversion efficiency of up to 86%.

■ ASSOCIATED CONTENT

Supporting Information

Experimental method, absorption spectra, solar cell parameters, and dark *J*−*V* curves. This material is available free of charge via the Internet at http://pubs.acs.org.

■ AUTHOR INFORMATION

Corresponding Authors

yixin.zhao@sjtu.edu.cn
Kai.Zhu@nrel.gov

Notes

The authors declare no competing financial interest.

■ ACKNOWLEDGMENTS

Y.Z. acknowledges the support of the NSFC (Grant 51372151). K.Z. acknowledges the support by the U.S. Department of Energy/National Renewable Energy Laboratory's Laboratory Directed Research and Development (LDRD) program under Contract No. DE-AC36-08GO28308.

■ REFERENCES

(1) Kojima, A.; Teshima, K.; Shirai, Y.; Miyasaka, T. *J. Am. Chem. Soc.* **2009**, *131*, 6050.
(2) Im, J.-H.; Lee, C.-R.; Lee, J.-W.; Park, S.-W.; Park, N.-G. *Nanoscale* **2011**, *3*, 4088.
(3) Kim, H.-S.; Lee, C.-R.; Im, J.-H.; Lee, K.-B.; Moehl, T.; Marchioro, A.; Moon, S.-J.; Humphry-Baker, R.; Yum, J.-H.; Moser, J. E.; Gratzel, M.; Park, N.-G. *Sci. Rep.* **2012**, *2*, 1.
(4) Burschka, J.; Pellet, N.; Moon, S. J.; Humphry-Baker, R.; Gao, P.; Nazeeruddin, M. K.; Gratzel, M. *Nature* **2013**, *499*, 316.
(5) Liu, M.; Johnston, M. B.; Snaith, H. J. *Nature* **2013**, *501*, 395.
(6) Kim, H.-S.; Im, S. H.; Park, N.-G. *J. Phys. Chem. C* **2014**, *118*, 5615.
(7) Snaith, H. J. *J. Phys. Chem. Lett.* **2013**, 3623.
(8) Christians, J. A.; Fung, R. C. M.; Kamat, P. V. *J. Am. Chem. Soc.* **2014**, *136*, 758.
(9) Lee, M. M.; Teuscher, J.; Miyasaka, T.; Murakami, T. N.; Snaith, H. J. *Science* **2012**, *338*, 643.
(10) Zhao, Y.; Nardes, A. M.; Zhu, K. *J. Phys. Chem. Lett.* **2014**, *5*, 490.
(11) Noh, J. H.; Im, S. H.; Heo, J. H.; Mandal, T. N.; Seok, S. I. *Nano Lett.* **2013**, *13*, 1764.
(12) Qiu, J.; Qiu, Y.; Yan, K.; Zhong, M.; Mu, C.; Yan, H.; Yang, S. *Nanoscale* **2013**, *5*, 3245.
(13) Edri, E.; Kirmayer, S.; Cahen, D.; Hodes, G. *J. Phys. Chem. Lett.* **2013**, 897.
(14) Edri, E.; Kirmayer, S.; Kulbak, M.; Hodes, G.; Cahen, D. *J. Phys. Chem. Lett.* **2014**, *5*, 429.
(15) Ryu, S.; Noh, J. H.; Jeon, N. J.; Chan Kim, Y.; Yang, W. S.; Seo, J.; Seok, S. I. *Energy Environ. Sci.* **2014**, *7*, 2614.
(16) Eperon, G. E.; Stranks, S. D.; Menelaou, C.; Johnston, M. B.; Herz, L. M.; Snaith, H. J. *Energy Environ. Sci.* **2014**, *7*, 982.
(17) Miles, R. W. *Vacuum* **2006**, *80*, 1090.
(18) Wehrenfennig, C.; Eperon, G. E.; Johnston, M. B.; Snaith, H. J.; Herz, L. M. *Adv. Mater.* **2013**, *26*, 1584.
(19) Zhao, Y.; Zhu, K. *J. Phys. Chem. C* **2014**, *118*, 9412.
(20) Eperon, G. E.; Burlakov, V. M.; Docampo, P.; Goriely, A.; Snaith, H. J. *Adv. Funct. Mater.* **2014**, *24*, 151.
(21) Chen, Q.; Zhou, H.; Hong, Z.; Luo, S.; Duan, H.-S.; Wang, H.-H.; Liu, Y.; Li, G.; Yang, Y. *J. Am. Chem. Soc.* **2014**, *136*, 622.
(22) Liu, D.; Kelly, T. L. *Nat. Photonics* **2014**, *8*, 133.
(23) Docampo, P.; Hanusch, F.; Stranks, S. D.; Döblinger, M.; Feckl, J. M.; Ehrensperger, M.; Minar, N. K.; Johnston, M. B.; Snaith, H. J.; Bein, T. *Adv. Energy Mater.* **2014**, DOI: 10.1002/aenm.201400355.
(24) Liang, P.-W.; Liao, C.-Y.; Chueh, C.-C.; Zuo, F.; Williams, S. T.; Xin, X.-K.; Lin, J.; Jen, A. K. Y. *Adv. Mater.* **2014**, *26*, 3748−3754.
(25) Dualeh, A.; Tétreault, N.; Moehl, T.; Gao, P.; Nazeeruddin, M. K.; Grätzel, M. *Adv. Funct. Mater.* **2014**, *24*, 3250.
(26) Choi, J. J.; Yang, X.; Norman, Z. M.; Billinge, S. J. L.; Owen, J. S. *Nano Lett.* **2014**, *14*, 127.
(27) Conings, B.; Baeten, L.; De Dobbelaere, C.; D'Haen, J.; Manca, J.; Boyen, H.-G. *Adv. Mater.* **2014**, *26*, 2041.
(28) Xiao, M.; Huang, F.; Huang, W.; Dkhissi, Y.; Zhu, Y.; Etheridge, J.; Gray-Weale, A.; Bach, U.; Cheng, Y.-B.; Spiccia, L. *Angew. Chem., Int. Ed.* **2014**, DOI: 10.1002/anie.201405334.
(29) Jeon, N. J.; Noh, J. H.; Kim, Y. C.; Yang, W. S.; Ryu, S.; Seok, S. I. *Nat. Mater.* **2014**, DOI: 10.1038/nmat4014.